Sustainable simultaneous synthesis of titanium-bearing materials from silicon waste and TiO_2-bearing slag

Chen, Zhiyuan; You, Yuliu; Morita, Kazuki

DOI
10.1021/acssuschemeng.8b02058

Publication date
2018

Document Version
Final published version

Published in
ACS Sustainable Chemistry and Engineering

ACS Sustainable Chemistry & Engineering

Research Article

Cite This: ACS Sustainable Chem. Eng. 2018, 6, 10742−10750

Sustainable Simultaneous Synthesis of Titanium-Bearing Materials from Silicon Waste and TiO_2-Bearing Slag

Zhiyuan Chen,*[,†,‡] Yuliu You,[†,‡] and Kazuki Morita[†]

[†]Department of Materials Engineering, Graduate School of Engineering, The University of Tokyo, Engineering, Building no. 4, 7-3-1 Hongo, Bunkyo-ku, Tokyo 113-8656, Japan

[‡]Department of Materials Science and Engineering, Delft University of Technology, Block H, Building 34, Mekelweg 2, Delft 2628, The Netherlands

ABSTRACT: A sustainable simultaneous synthesis method of TiB_2−Ti_5Si_3 mixtures is developed as an alternative recovery route of silicon waste from the photovoltaics industry. TiO_2−CaO−B_2O_3 ternary was reduced by molten silicon at 1500 °C, producing TiB_2 within 3 h and Ti_5Si_3 within 10 h. The lab-scale experiments were designed to study the reaction kinetics of the reaction. SiO_2 diffusion rate controlling kinetic model was derived to describe the reaction process. The reaction rate constant was recommended to be $\sim 5 \times 10^{-4}$ s^{-1}. B_2O_3 content in slag was suggested to have an insignificant effect on the reaction rate constant, whereas more titanium and boron could be reduced by silicon with higher B_2O_3 content in slag. Stability of the reaction interface was simulated using phase field model. A decreased interfacial tension in B_2O_3-containing system was indicated to be the reason for emulsification of phases.

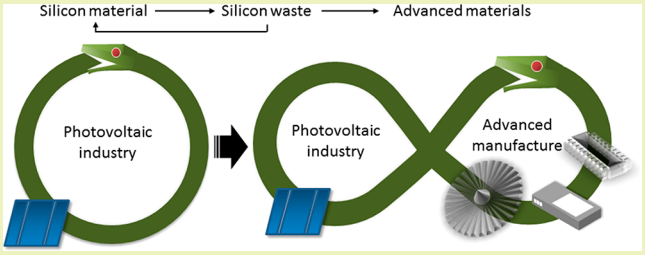

KEYWORDS: *Titanium diboride, Titanium silicide, Synthesis kinetics, Photovoltaic, Silicon waste*

INTRODUCTION

The rapid growth of the photovoltaic (PV) industry over the last few decades has caused an exponential increase in silicon waste. Therefore, silicon waste recycling is becoming a more and more important issue and drawing a great amount of attention from researchers all over the world.[1,2] The recycling issue in the PV industry gets serious nowadays because of the exponential increase in waste.[3,4] Silicon wastes include end-of-life solar cells,[5,6] off-spec silicon,[7] and so on.[8] These silicon wastes are expected to be recycled in the PV industry to maximize the silicon profitability. Abundant processes are practiced to establish a closed-loop life cycle for silicon wastes.[5,9] Meanwhile, recently, an alternative strategy to reuse silicon wastes as other advanced materials has been raised as a necessary complement of a feasible recycling pathway. For instance, Xiang et al.[10] synthesized silicon-based anode material from silicon cutting kerf loss for lithium-ion battery. Moreover, silicon carbide, another reusable material from silicon wafer slicing slurry, was also recovered as photocatalysts.[11]

The importance of developing alternative approaches out of the closed-loop recycling of silicon wastes in the PV industry is basically for the economic reason. The market price of silicon ingot/wafer has a significant effect on the profitability of the closed-loop cycle in the PV industry.[12] Several researchers[13−15] already claimed that recycling silicon wastes in the PV industry is economically unfavorable without appropriate incentives of policies. To protect investments in silicon recycling industry and encourage development of sustainable solar technologies, it is critical to explore alternative, facile, and profitable recycling/recovery processes. These processes can also connect the PV industry with other manufacturing industries, which would be an important step toward a circular economy in a wider scope.

The aim of this work is to study the possibility of simultaneous synthesis of TiB_2 and Ti_5Si_3 powders from the silicon waste in the aspect of chemical reaction kinetics. Titanium diboride, TiB_2, is an increasingly important refractory material with high melting point (2790 °C) and high resistance to plastic deformation at high temperature.[16] It is also an advanced engineering ceramic.[17] Similarly, Ti_5Si_3 is one of the promising refractory materials with multiple uses.[18] Both Ti_5Si_3[19] and TiB_2[20] are used to improve the microstructure and enhance the mechanical properties[21] of TiAl matrix composites. Specifically, Qiu et al.[22] reported that TiB_2 and Ti_5Si_3 in dual-phase nanoparticles can refine the grain size of TiAl alloy and enhance the comprehensive compression properties of TiAl composites. Zhang et al.[23] also found that the mechanical property of TiN−TiB_2 can be improved with the addition of Ti_5Si_3. Besides Ti_5Si_3, $TiSi_2$ added to TiB_2 composites can exhibit an excellent combination of properties.[24−26] Other than that, $TiSi_2$−TiB_2 was reported as a layered coating of chromium to protect it from reaction with

Received: May 4, 2018
Revised: June 25, 2018
Published: June 29, 2018

DOI: 10.1021/acssuschemeng.8b02058
ACS Sustainable Chem. Eng. 2018, 6, 10742−10750

Table 1. Compositions and Weights of Slags Used in the Experiments[a]

	slag composition/mass%						
no.	CaO	TiO_2	B_2O_3	surface tension/mN·m^{-1}	solidus/liquidus temperature/K	density of slag/g·cm^{-3}	viscosity of slag/mPa·s
1	18.5	81.5	0.0	426	1722/1802	3.19	169
2	17.5	77.3	5.2	278	1293/1667	3.07	163
3	16.7	73.8	9.5	253	1293/1667	2.97	158
4	15.9	70.3	13.8	246	1293/1651	2.89	155

[a]Experiments at different reaction times are in progress.

air at high temperature.[27] All these research studies show that Ti_5Si_3−TiB_2 and $TiSi_2$−TiB_2 mixtures are promising materials.

Usually, the two refractory materials are synthesized from the mixtures of monoatomic powders.[28−30] Another commercialized method to produce TiB_2 powders is the carbothermal reduction of B_4C,[31,32] B_2O_3,[33] H_3BO_3, or HBO_2,[34] and CO is released as a byproduct. In the past few years, mechanical activation[35] was introduced to decrease the reaction temperature. Other reductants other than carbon were also studied, such as Mg[36−38] and Al.[39] Recently, Nozari et al.[40] developed a facile synthesis method of TiB_2 particles through the reaction of

$$TiO_2 + B_2O_3 + 2.5Si = TiB_2 + 2.5SiO_2 \quad (1)$$

Moreover, a sustainable synthesis method of Ti_5Si_3 from molten silicon and TiO_2-bearing slag was reported in our recent work.[41−43] Slag from the steelmaking process and silicon waste from the fast-developing photovoltaics industry can be recovered to produce refractory materials by this method. In the present work, we proposed a method that combines the synthesis of TiB_2 and Ti_5Si_3 materials using molten silicon and B_2O_3−TiO_2−CaO ternary as precursors. The composition of the ternary was also studied to understand the effect of B_2O_3 content on the reaction kinetics.

MATERIALS AND METHODS

Materials and Methods. Certain amounts of CaO, TiO_2, and B_2O_3 were mixed and premelted at 1773 K to form slag. Molten silicon (0.6 g) was placed in a high-purity graphite crucible with 8 mm inner diameter, and 2.11 g of slag floated on the surface of the molten silicon. The reaction time ranged from 3 to 15 h in argon atmosphere at 1773 K. In the practical synthesis process, the molten silicon floats on the surface of the slag and the heavy intermetallic product droplets precipitate through the slag and deposit on the bottom of the high-temperature reactor. Reaction occurs at the interfaces of silicon−slag and falling droplets−slag. Therefore, the reaction interface is expanded by the formation of large amount of droplets, and hence the reaction is accelerated. However, to quantitatively study the reaction kinetics, a stable reaction interface is required. Therefore, in this study, the initial position of slag and silicon was exchanged, i.e., slag maintains on the molten silicon, to avoid the precipitation of intermetallic droplets in slag, obtain a stable reaction interface, and, hence, simplify the kinetic analysis.[43]

Some important physical properties of the slag are listed in Table 1. The surface tension and density of slag are estimated using Mills' model[44] combined with the calculation results of liquidus temperature of the slag via FactSage 7.0. Viscosity data was estimated by FactSage 7.0. The density of molten silicon is 2.56 g cm^{-3}.[45] The density difference between molten silicon and slag forms a driving force for the floating of silicon. It is expected that the relative positions of slag and molten silicon can remain stable. The stable interfacial area is beneficial for kinetic analysis. A simplified relationship between viscosity and stability of slag−silicon interface will be introduced in the following section.

Characterization. After the reaction, the sample was withdrawn from the furnace, quenched in argon gas, and subjected to characterization. The X-ray diffraction (XRD, Rigaku Rint-2100) analysis, optical microscope, and scanning electron microscope (JSM-6510LA, JEOL Ltd.) equipped with energy-dispersive spectroscopy (SEM/EDS) observation were conducted on the reaction products. Moreover, to quantitatively study the kinetics, inductively coupled plasma atomic emission spectroscopy (ICP-AES, SPS 7700, SII Nano Technology, Japan) was employed to analyze the composition of quenched slag. For ICP-AES analysis, 0.5 g of Na_2CO_3 and 0.5 g of $Na_2B_4O_7$ were used for digestion of 0.1 g of crushed slag in a Pt crucible at 1273.15 K for 20 min. Then the alkaline fused sample was dissolved in 1:3 HCl/H_2O acid solution. The accuracy of this method has been approved by detection of the original slag before reaction.[43] To simulate variation of the slag−silicon interface area in the reaction, Comsol Multiphysics 5.3 was employed in the analysis.

RESULTS AND DISCUSSION

Reaction Products. Figure 1 shows the typical products in the silicon−slag reaction process. TiO_2 could be reduced to suboxides, such as Ti_2O_3. Besides, TiB_2 and Ti_5Si_3 were observed as products after reaction for 3 and 10 h, respectively. EDS analysis was employed to verify the components of the

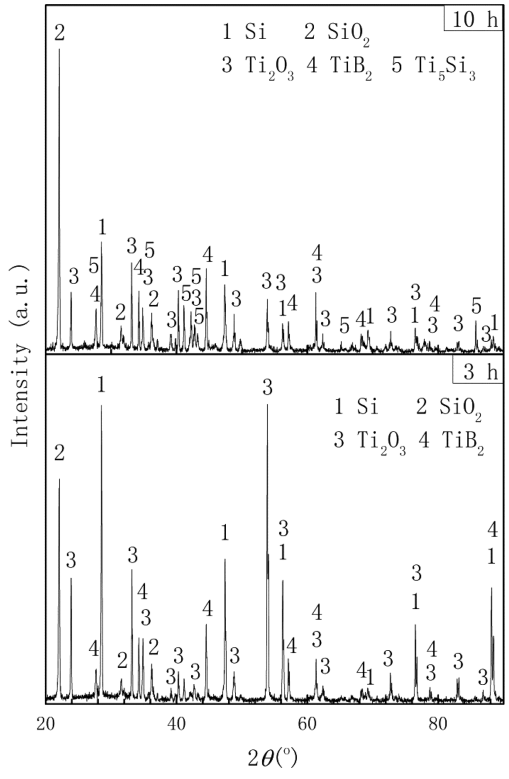

Figure 1. XRD patterns of ground products made from slag no. 4 (13.8 mass % B_2O_3) after reaction for 3 and 10 h at 1773 K, respectively.

DOI: 10.1021/acssuschemeng.8b02058
ACS Sustainable Chem. Eng. 2018, 6, 10742−10750

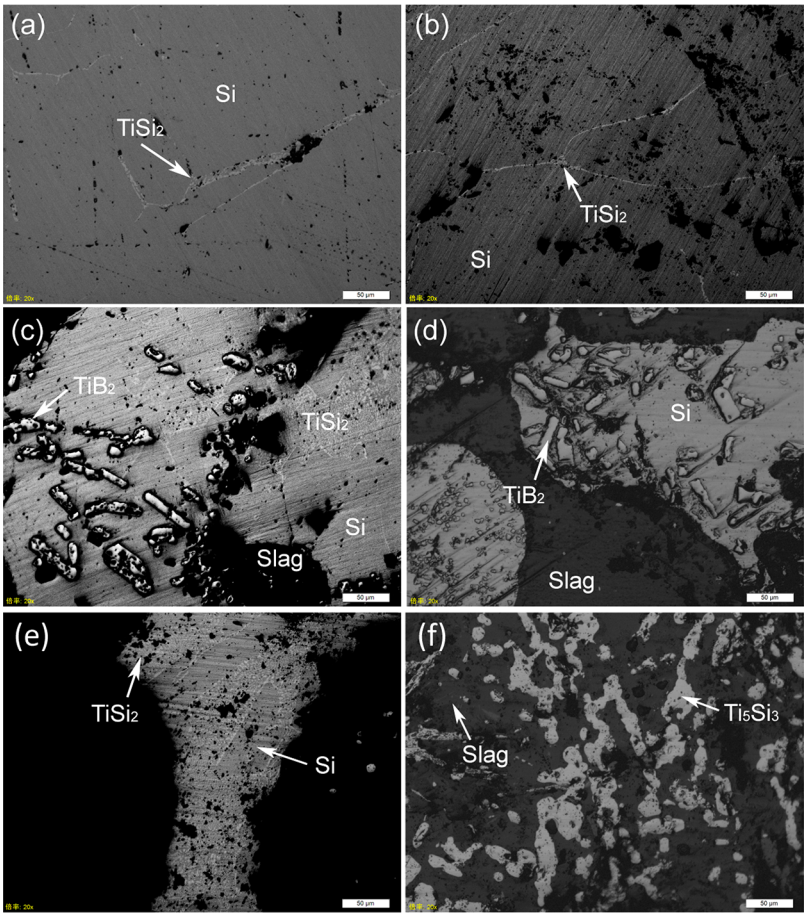

Figure 2. Microstructure of samples (a) without B_2O_3 in slag and reacted for 3 h, (b) without B_2O_3 in slag and reacted for 10 h, and (c) with 13.8 mass % B_2O_3 in slag and reacted for 3 h, (d–f) with 13.8 mass % B_2O_3 in slag and reacted for 10 h at 1773 K.

compounds. Components Ti and Si can be detected in both Ti_5Si_3 and $TiSi_2$; however, only Ti can be detected in TiB_2 due to the limitation of EDS technology. For instance, the detection result of $TiSi_2$ is Ti/Si = 42.85:57.15 in mass ratio; Ti_5Si_3 is Ti/Si = 76.93:23.07 in mass ratio. The previous study indicates that the reaction between B_2O_3-free slag and silicon could only produce $TiSi_2$ and Ti_5Si_3.[41,42] Parts a and b of Figure 2 suggest the same results: $TiSi_2$ was generated at the boundary of silicon crystals during the solidification, which was not detected by XRD because of the extremely low amount. In the reaction between slag no. 4 (13.8 mass % B_2O_3) and molten silicon, lots of TiB_2 micrograins formed within the molten silicon. Unlike the sintered Ti_5Si_3 skeleton structure, TiB_2 forms as dispersive grains due to its high melting point. The densities of B_2O_3, Ti_5Si_3, and $TiSi_2$ are 4.52, 4.32, and 4.07 $g\cdot cm^{-3}$, respectively.[46] Because of the density difference between molten silicon (2.56 $g\cdot cm^{-3}$)[47] and molten slag, the products could be separated naturally. To accelerate the separation progress, supergravity technology[48] can be a promising method. It is known from a previous study[41,42] that the reaction between TiO_2 in slag and molten silicon could produce Ti_5Si_3 in three steps as shown in eqs 2–4.

$$(TiO_2) + [Si] = [Ti] + (SiO_2) \quad K_{(1)} = 2.88\ (1500\ ^\circ C) \tag{2}$$

$$[Ti] + 2[Si] = TiSi_2 \quad K_{(2)} = 2.81 \times 10^3\ (1500\ ^\circ C) \tag{3}$$

$$7[Ti] + 3TiSi_2 = 2Ti_5Si_3 \quad K_{(3)} = 1.09 \times 10^{19}\ (1500\ ^\circ C) \tag{4}$$

where K represents the reaction equilibrium constant of the reaction. Additionally, boron can be reduced from slag into silicon solution. The combination of the reactions presented in eqs 2 and 5 produces Ti–B–Si ternary and then generates TiB_2.

$$2(B_2O_3) + 3[Si] = 4[B] + 3(SiO_2) \quad K_{(4)} = 3.28\ (1500\ ^\circ C) \tag{5}$$

$$[Ti] + 2[B] = TiB_2 \quad K_{(5)} = 1.01 \times 10^8\ (1500\ ^\circ C) \tag{6}$$

The values of the reaction equilibrium constants are quite small in eqs 2 and 5, which indicates that the two reactions are reversible reactions. It is known that

$$K = \frac{k_f}{k_b} \tag{7}$$

where k_f represents the reaction rate constant in the forward direction and k_b represents the reaction rate constant in the backward direction. Relatively high values of K in eqs 3, 4, and 6 imply high reaction rates in the forward direction, k_f, of these chemical reactions compared to the other two equations. Therefore, we could assume that only the kinetic steps directly related to the chemical reaction of eqs 2 and 5 could be the

DOI: 10.1021/acssuschemeng.8b02058
ACS Sustainable Chem. Eng. 2018, 6, 10742–10750

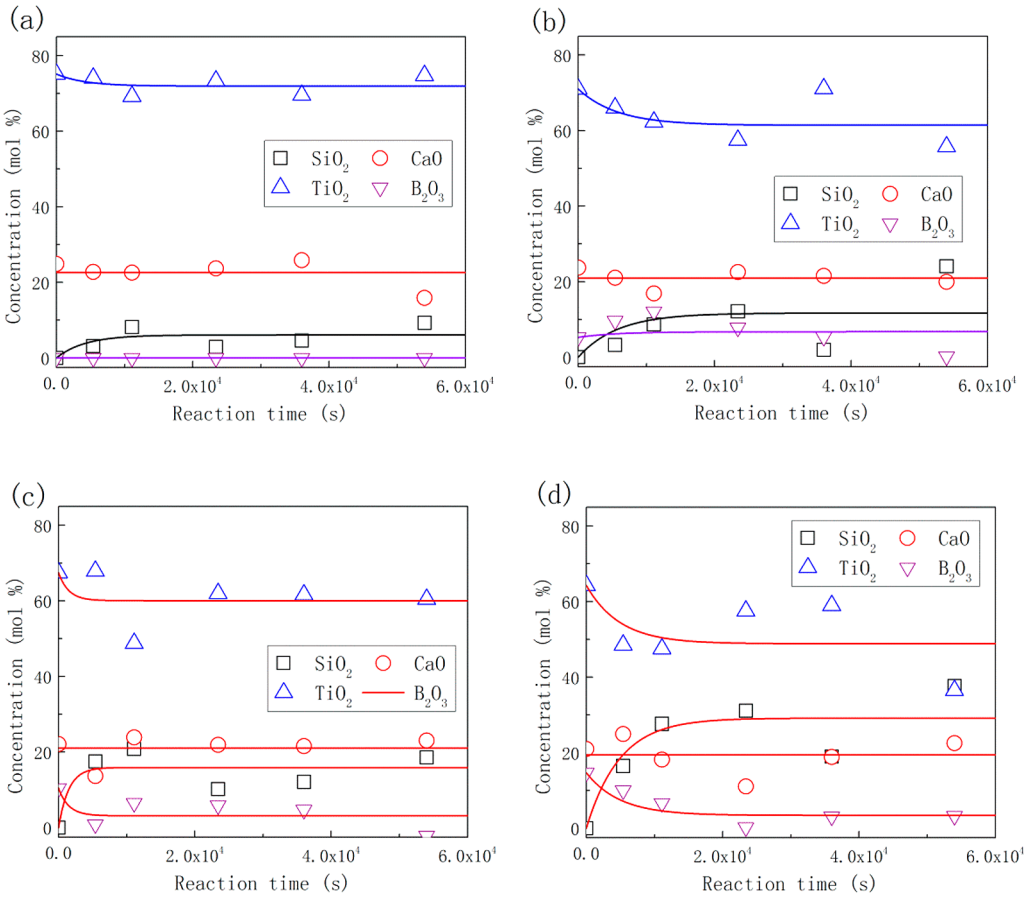

Figure 3. Slag composition variation during the reaction with molten silicon at 1773 K in Ar atmosphere with initial boron concentration as (a) 0; (b) 5.2 mass %; (c) 9.5 mass %; and (d) 13.8 mass % (the curves are the fitting results of eqs 11, 14, and 15, respectively).

possible reaction rate-determining step. Commonly, chemical reaction could not be the slowest step in such a high-temperature process. Moreover, the diffusion in the slag is approximately an order of magnitude faster than that in molten metal.[49] Therefore, based on the study of titanium silicide synthesis,[43] diffusion of SiO_2 from the reaction interface to the slag bulk phase could be the reaction rate-determining step.

Kinetic Model. Transport of SiO_2 in the slag diffusion layer was suggested to be the rate-determining step of the reaction.

$$\frac{dn_{SiO_2}}{dt} = Ak_{SiO_2}(x_{(SiO_2)_i} - x_{SiO_2}) \tag{8}$$

where n_{SiO_2} is the amount of SiO_2; t is the reaction time; A is the reaction interface, which is assumed to be constant (0.005 m^2) in the reaction; k_{SiO_2} is the diffusion constant; $x_{(SiO_2)_i}$ and x_{SiO_2} are the concentrations of SiO_2 at the interface and within the slag, respectively.

$$n_{SiO_2} = x_{SiO_2} n_{slag} \tag{9}$$

where n_{slag} is the amount of slag. Combining eqs 8 and 9,

$$\frac{dx_{SiO_2}}{dt} = \frac{A}{n_{slag}} k_{SiO_2}(x_{(SiO_2)_i} - x_{SiO_2}) \tag{10}$$

in terms of integration,

$$\ln \frac{x_{SiO_2} - x_{(SiO_2)_i}}{x_{(SiO_2)_0} - x_{(SiO_2)_i}} = -\frac{A}{n_{slag}} k_{SiO_2} t \tag{11}$$

where the 0 as subscript presents the initial state ($t = 0$) and $x_{(SiO_2)_0} = 0$. It could be turned into the function of x_{TiO_2},

$$\ln \frac{x_{TiO_2} - (1 - x_{CaO} - x_{(B_2O_3)_i} - x_{(SiO_2)_i})}{x_{(TiO_2)_0} - (1 - x_{(CaO)_0} - x_{(B_2O_3)_0} - x_{(SiO_2)_i})} = \frac{A}{n_{slag}} k_{SiO_2} t \tag{12}$$

where

$$x_{(TiO_2)_i} + x_{(SiO_2)_i} + x_{(B_2O_3)_i} + x_{(CaO)_i} = x_{TiO_2} + x_{SiO_2} + x_{B_2O_3} + x_{CaO} = 1 \tag{13}$$

Furthermore, $x_{(CaO_2)_i}$ is a constant during the entire experiment and is equal to x_{CaO}. Therefore, combined with eq 13, eq 12 becomes

$$\ln \frac{x_{TiO_2} - x_{(TiO_2)_i}}{x_{(TiO_2)_0} - x_{(TiO_2)_i}} = \frac{A}{n_{slag}} k_{SiO_2} t \tag{14}$$

Similarly,

$$\ln \frac{x_{B_2O_3} - x_{(B_2O_3)_i}}{x_{(B_2O_3)_0} - x_{(B_2O_3)_i}} = \frac{A}{n_{slag}} k_{SiO_2} t \tag{15}$$

DOI: 10.1021/acssuschemeng.8b02058
ACS Sustainable Chem. Eng. 2018, 6, 10742−10750

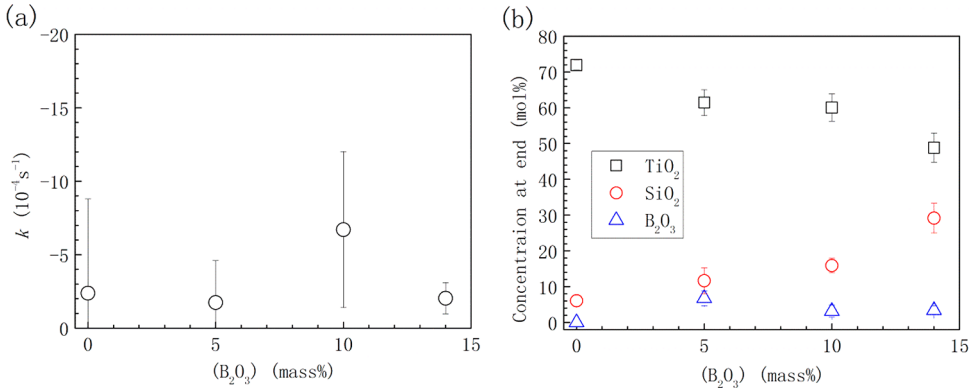

Figure 4. Kinetic parameters in eqs 11, 14, and 15 to describe the reaction of titanium-bearing slag with molten silicon at 1773 K in Ar atmosphere: (a) reaction rate constant k and (b) final concentration of oxides.

When modeling the experimental data, $x_{(\text{oxide})_i}$ was replaced by a parameter, $x_{(\text{oxide})_e}$, that represents the terminal oxide content in the slag in the reaction.

It could be noticed that the chemical equilibrium constant of eq 2 is as follows:

$$K_{(1)} = \frac{x_{(SiO_2)_i} x_{Ti}}{x_{(TiO_2)_i} x_{Si}} \tag{16}$$

Similarly,

$$K_{(4)} = \frac{x_{(SiO_2)_i}^{3} x_B^{4}}{x_{(B_2O_3)_i}^{2} x_{Si}^{3}} \tag{17}$$

Moreover,

$$K_{(2)} = \frac{1}{x_{Ti}(x_{Si})^2} \tag{18}$$

and

$$K_{(5)} = \frac{1}{x_{Ti}(x_B)^2} \tag{19}$$

where

$$x_{Ti} + x_{Si} + x_B = 1 \tag{20}$$

Combining eqs 18−20, one could get the following numerical solution:

$$x_{Ti} = 3.59 \times 10^{-4};\ x_{Si} = 0.994;\ x_B = (5.26 \pm 0.40) \times 10^{-3} \tag{21}$$

Combining eqs 16 and 17 yields

$$(x_{Ti} + K_{(1)} x_{Si}) x_{(SiO_2)_i} + \frac{x_B x_{(SiO_2)_i}^{3/2} K_{(1)}}{x_{Si}^{1/2} K_{(4)}^{1/2}} = K_{(1)} x_{Si} (1 - x_{CaO}) \tag{22}$$

Because $(x_{Ti} + K_{(1)}x_{Si}) \approx K_{(1)}x_{Si} >> \frac{x_B K_{(1)}}{x_{Si}^{1/2} K_{(4)}^{1/2}}$, eq 22 could be simplified as

$$x_{(SiO_2)_i} \approx 1 - x_{CaO} \tag{23}$$

This indicates that B_2O_3 and TiO_2 in slag could be completely extracted from slag in an ideal condition.

Reaction Kinetics. Compared to the alloy part, slag could be treated as a homogeneous phase after quenching. Therefore, investigation of chemical composition variation of the slag phase is suitable for kinetic analysis of TiB_2 and Ti_5Si_3 synthesis. Figure 3 shows the chemical analysis results of the reaction. Equations 11, 14, and 15 were employed for kinetic modeling of experimental results. The experimental error of the B_2O_3-containing experiments is obvious. One of the important reasons is that the vapor pressure of B_2O_3 is relatively high compared to those of other compounds. Attention has been paid to the evaporation of B_2O_3 from the melts. For instance, Wang et al.[50] used 30 g of slag in a crucible with 40 mm inner diameter. The B_2O_3 content decreased by ∼0.3−0.6 mass % of the total slag in the high-temperature operation. Zhang et al.[51] studied the evaporation kinetics of B_2O_3 in melts. Their experimental results show that the range of mass loss is from 0.5 to 7 mass % in various conditions. The crucibles with small inner diameter are used in our experiments to prevent the serious mass loss of slag by evaporation. Moreover, introduction of B_2O_3 causes a sharp decrease of surface tension of slag, resulting in a mixture of slag and molten silicon. Hence, some silicon or intermetallic droplets could be taken into the analysis of slag samples.

The reaction rate constant and the final concentration of oxides can also be obtained from the fitting curves, which are shown in Figure 4. The reaction rate constant of the process is around -5×10^{-4} s^{-1}. Figure 4a shows that adding B_2O_3 could not efficiently raise the reaction rate constant. This implies that the diffusion rate of SiO_2 in B_2O_3-containing slag is not accelerated. This could be due to the fact that the viscosity of the slag does not change much with addition of B_2O_3.[43] Moreover, it also indicates that, although the B_2O_3 evaporation reduces the B resource for the reaction and further reduces the yield of TiB_2, it has no significant effect on the reaction rate constant. Nevertheless, more TiO_2 could be extracted out from slag with increasing B_2O_3 content in slag. Correspondingly, the final SiO_2 content in the slag increased. The results suggest that high B_2O_3 content is beneficial to the utilization of silicon. B_2O_3 content at the reaction end also decreased from 6.76 ± 2.09 to 3.15 ± 1.65 mol % with an increase of initial B_2O_3 content from 5.2 to 9.5 mass %. A further increase of initial B_2O_3 content did not change the final B_2O_3 content. Although the thermodynamic calculation result implies that B_2O_3 and TiO_2 in the slag could be converted into TiB_2 and titanium silicides, the residual B_2O_3 and TiO_2 in the slag at the reaction end deviated from the equilibrium state. This could be due to

DOI: 10.1021/acssuschemeng.8b02058
ACS Sustainable Chem. Eng. 2018, 6, 10742−10750

the fact that silicon was surface-active in the slag,[52] which blocked further interfacial reactions.

Stability of the Interface. Figure 5 shows the longitudinal section of the samples reacted for 3 h at 1773 K. Molten silicon

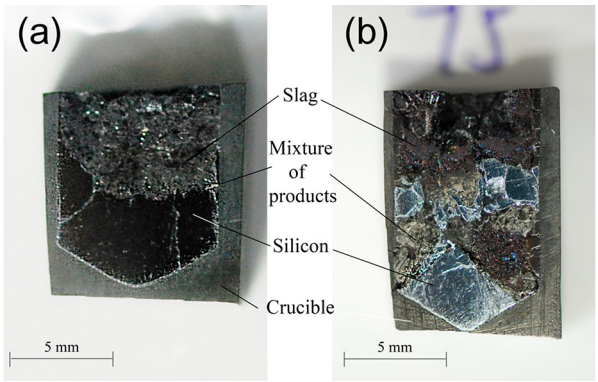

Figure 5. Longitudinal section of the reacted samples (a) without B_2O_3 in the slag and (b) with 5.2 mass % B_2O_3 in the slag after reaction for 3 h at 1773 K.

shows better wettability to the graphite wall compared with slag, which turns the shape of the interface into a meniscus. Even so, the relative position of silicon and slag remained the same as the initial state as shown in Figure 5a. With 5.2 mass % B_2O_3 addition in the slag, the estimated viscosity of the slag decreased from 169 to 163 mPa·s, and the surface tension of the slag decreased from 426 to 278 mN·m^{-1}. In this case, molten silicon floated up in the experiment. During the floating up, molten silicon was separated into several parts, and many tiny droplets formed and dispersed in the slag phase. Figure 5b shows the emulsification of silicon in the slag within the crucible. The drastic variation of interface area during the reaction resulted in unstable apparent reaction rate constant as shown in Figure 4a.

To illustrate the effect of slag properties on the stability of the slag–silicon interface, a two-dimensional simulation was carried out with the finite element software Comsol Multiphysics 5.3. Navier–Stokes equations and the continuity equation are involved for the conservation of momentum and mass, respectively. The system was assumed as a laminar-flow regime considering the wetting wall boundary condition. Gravity was introduced as a body force. Allen–Cahn phase field model was employed for identification of phases, where a diffuse interface separates the slag and molten silicon phases.[53] The phase field varies toward the direction along which the fluid free energy of the system was minimized. The fluid free energy density is described by the equation

$$F(C) = \int_{\Omega} \left\{ \frac{1}{2}\alpha|\vec{\nabla}C|^2 + \beta\Psi(C) \right\} \mathrm{d}C \tag{24}$$

where C is the dimensionless phase-field variable, Ω represents the region of simulated space, the two terms in the brace are gradient energy and bulk energy in sequence, and $\Psi(C)$ models the immiscibility of fluid components, which has two minima corresponding to two stable phases. $O\sqrt{\alpha/\beta}$ is the width separating two phases and is assumed to be half of the mesh element size at the interface, and $\sqrt{\alpha\beta}$ is proportional to the interfacial tension.

First of all, the physical parameters of the melts should be provided for the simulation. Viscosity of fluid is a key parameter in the Navier–Stokes equation, and interfacial tension is required for the phase-field model. The viscosity of molten silicon at 1773 K was estimated as 0.767 mPa·s based on the equation of Sato et al.[54] Surface tension of molten silicon at 1773 K was suggested to be 729 mN·m^{-1} based on the work of Fujii et al.[55]

The viscosity of the slag is listed in Table 1, and it slightly decreases with increasing B_2O_3 content in the slag. The error of estimated value of viscosity is small when referring to the experimental data of slag with similar compositions,[56] and the tendency of viscosity is similar to the reported data. For instance, Ren et al.[57] show that the viscosity of slag decreases from 286 to 238 mPa·s with B_2O_3 content in slag increasing from 0 to 4.1 mass % at 1773 K. Although the increase of viscosity with B_2O_3 content is obvious at lower temperature,[58] the effect of the slag component on the viscosity variation can be reduced at temperatures above a certain breaking point.

On the basis of the approach of Girifalco and Good, the interfacial tension $\gamma_{\text{slag-silicon}}$ could be calculated from the surface tension of slag (γ_{slag}) and silicon (γ_{silicon}),[59]

$$\gamma_{\text{slag-silicon}} = \gamma_{\text{slag}} + \gamma_{\text{silicon}} - 2\Phi\sqrt{\gamma_{\text{slag}}\gamma_{\text{silicon}}} \tag{25}$$

where the interaction coefficient Φ varies from 1 to 0. However, there is no widely applicable model to estimate the value of Φ for the silicon–slag interface. It is assumed that the increase of B_2O_3 content could reduce the interfacial tension of the silicon–slag interface. Two typical values of interfacial tension, 60 mN·m^{-1} for B_2O_3-free slag and 30 mN·m^{-1} for B_2O_3-containing slag, were adopted in this simulation based on this assumption.

The wetting angles of silicon and B_2O_3-free slag on graphite were assumed as 20°[60] and 100°,[61,62] respectively. Correspondingly, the contact angle of silicon on graphite crucible is 131° with a three-phase boundary of silicon–slag–graphite.

The computation was made on the domain with 35 mm in height and 8 mm in width. It was meshed with 5×10^4 quad/triangular mixed elements. Only slag and silicon phases were contained in the system. At the initial stage, slag floats on the molten silicon phase. The influence of heat transfer and chemical reactions were ignored. Backward differentiation formula was employed for time stepping. In the simulation, the conditions with different values of slag viscosity and interfacial tension were compared as shown in Figure 6. It shows that the interface remains stable when the interfacial tension is 60 mN·m^{-1} for B_2O_3-free slag. No velocity vectors are presented in the domain, which implies that the system reaches equilibrium state. Meanwhile, the systems with interfacial tension of 30 mN·m^{-1} have not reached the equilibrium state. Weak interfacial tension results in floating up of silicon phase through molten slag. The increasing fluidity of slag can promote the movement of slag–silicon interface. The simulation results indicate that B_2O_3 results in low interfacial tension of the slag–silicon interface, which causes emulsification of silicon in slag in the reaction.

CONCLUSIONS

Simultaneous synthesis of TiB_2 and Ti_5Si_3 was studied at 1500 °C. This process is recommended as a promising recovery method of silicon waste from the photovoltaics industry. CaO–TiO_2–B_2O_3 slag reacts with molten silicon, producing

DOI: 10.1021/acssuschemeng.8b02058
ACS Sustainable Chem. Eng. 2018, 6, 10742–10750

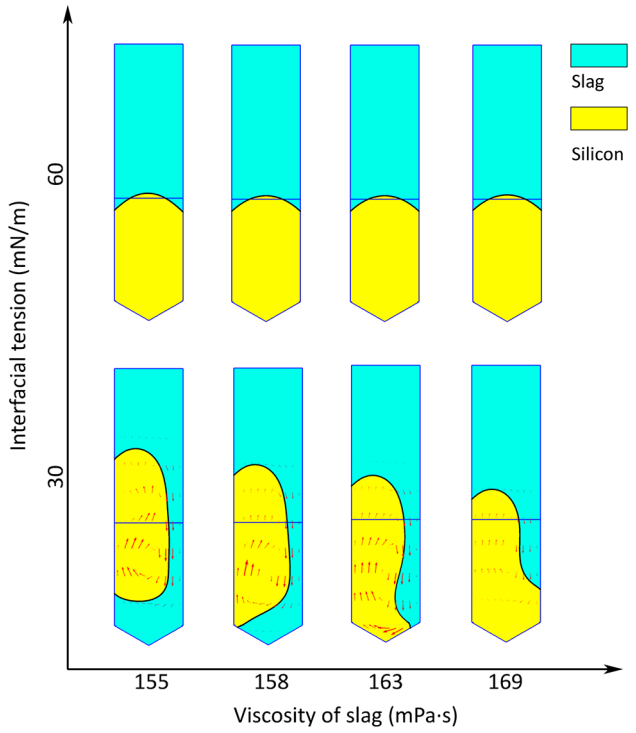

Figure 6. Simulation of silicon−slag interface with different interfacial tensions and viscosities at the same time, where the black bold curve represents the slag−silicon interface, fine lines are the initial interface and the inner wall of the crucible, and arrows represent the velocity vectors.

TiB_2 and Ti_5Si_3 within 3 and 10 h, respectively. The reductions of B_2O_3 and TiO_2 from the slag to form Ti and B solutes in silicon are recommended as reversible reactions. Diffusion of SiO_2 in slag bulk phase is the rate-determining step of the reaction kinetics. As a result, enrichment of SiO_2 at the reaction interface retards the reactions in the experiments. A kinetic model was developed for quantitative analysis. The analysis results suggest that the B and Ti in the slag could be completely extracted if the reaction could reach the equilibrium. Moreover, the reaction rate constant is proposed to be -5×10^{-4} s^{-1}. The experimental results show that the B_2O_3 content in slag has insignificant influence on the reaction rate constant. With the increases of B_2O_3 content from 0 to 13.8 mass %, not only does the extraction ratio of both Ti and B from the slag increase but also the SiO_2 content in the slag increases from 6 to 29 mol %. B_2O_3 causes an unstable slag−silicon interface. The simulation results imply that the high B_2O_3 content in the slag could decrease the interfacial tension, which is the reason for emulsification of silicon in slag. The low viscosity of B_2O_3-containing slag speeds up the emulsification process. It is indicated that further design of slag composition is needed to reduce the negative effect of SiO_2 and B_2O_3 in the future.

AUTHOR INFORMATION

Corresponding Author

*E-mail: aha_c@126.com, Z.Chen-5@tudelft.nl. Tel.: +31(0) 15 27 82307.

ORCID

Zhiyuan Chen: 0000-0002-7993-7386

Funding

This research did not receive any specific grant from funding agencies in the public, commercial, or not-for-profit sectors.

Notes

The authors declare no competing financial interest.

ACKNOWLEDGMENTS

The experimental and modeling works of this research were carried out at The University of Tokyo and TU Delft, respectively. Z.C. and Y.Y. formerly worked at the University of Tokyo and now work at TU Delft. The authors express our thanks to Dr. Sakae Shirayama, Hisao Kimura, and Naomi Nakaya from The University of Tokyo for their help and assistance in the study.

REFERENCES

(1) Sarti, D.; Einhaus, R. Silicon feedstock for the multi-crystalline photovoltaic industry. *Sol. Energy Mater. Sol. Cells* **2002**, *72*, 27−40.

(2) Xu, Y.; Li, J.; Tan, Q.; Peters, A. L.; Yang, C. Global status of recycling waste solar panels: A review. *Waste Manage. (Oxford, U. K.)* **2018**, *75*, 450−458.

(3) Savvilotidou, V.; Antoniou, A.; Gidarakos, E. Toxicity assessment and feasible recycling process for amorphous silicon and CIS waste photovoltaic panels. *Waste Manage. (Oxford, U. K.)* **2017**, *59*, 394−402.

(4) Huang, W.-H.; Shin, W. J.; Wang, L.; Sun, W.-C.; Tao, M. Strategy and technology to recycle wafer-silicon solar modules. *Sol. Energy* **2017**, *144*, 22−31.

(5) Shin, J.; Park, J.; Park, N. A method to recycle silicon wafer from end-of-life photovoltaic module and solar panels by using recycled silicon wafers. *Sol. Energy Mater. Sol. Cells* **2017**, *162*, 1−6.

(6) Paiano, A. Photovoltaic waste assessment in Italy. *Renewable Sustainable Energy Rev.* **2015**, *41*, 99−112.

(7) Woditsch, P.; Koch, W. Solar grade silicon feedstock supply for PV industry. *Sol. Energy Mater. Sol. Cells* **2002**, *72*, 11−26.

(8) Wang, T. Y.; Lin, Y. C.; Tai, C. Y.; Sivakumar, R.; Rai, D. K.; Lan, C. W. A novel approach for recycling of kerf loss silicon from cutting slurry waste for solar cell applications. *J. Cryst. Growth* **2008**, *310*, 3403−3406.

(9) Tao, J.; Yu, S. Review on feasible recycling pathways and technologies of solar photovoltaic modules. *Sol. Energy Mater. Sol. Cells* **2015**, *141*, 108−124.

(10) Xiang, K.; Wang, X.; Chen, M.; Shen, Y.; Shu, H.; Yang, X. Industrial waste silica preparation of silicon carbide composites and their applications in lithium-ion battery anode. *J. Alloys Compd.* **2017**, *695*, 100−105.

(11) Zhang, Y.; Hu, Y.; Zeng, H.; Zhong, L.; Liu, K.; Cao, H.; Li, W.; Yan, H. Silicon carbide recovered from photovoltaic industry waste as photocatalysts for hydrogen production. *J. Hazard. Mater.* **2017**, *329*, 22−29.

(12) Choi, J.-K.; Fthenakis, V. Crystalline silicon photovoltaic recycling planning: macro and micro perspectives. *J. Cleaner Prod.* **2014**, *66*, 443−449.

(13) McDonald, N. C.; Pearce, J. M. Producer responsibility and recycling solar photovoltaic modules. *Energy Policy* **2010**, *38*, 7041−7047.

(14) Sener, C.; Fthenakis, V. Energy policy and financing options to achieve solar energy grid penetration targets: Accounting for external costs. *Renewable Sustainable Energy Rev.* **2014**, *32*, 854−868.

(15) Cucchiella, F.; D'Adamo, I.; Rosa, P. End-of-Life of used photovoltaic modules: A financial analysis. *Renewable Sustainable Energy Rev.* **2015**, *47*, 552−561.

(16) Ramberg, J. R.; Wolfe, C. F.; Williams, W. S. Resistance of Titanium Diboride to High-Temperature Plastic Yielding. *J. Am. Ceram. Soc.* **1985**, *68*, C-78−C-79.

DOI: 10.1021/acssuschemeng.8b02058
ACS Sustainable Chem. Eng. 2018, 6, 10742−10750

(17) Wang, W.; Fu, Z.; Wang, H.; Yuan, R. Influence of hot pressing sintering temperature and time on microstructure and mechanical properties of TiB_2 ceramics. *J. Eur. Ceram. Soc.* **2002**, *22*, 1045−1049.
(18) Zhang, L.; Wu, J. Ti_5Si_3 and Ti_5Si_3-based alloys: Alloyingbehavior, microstructure and mechanical property evaluation. *Acta Mater.* **1998**, *46*, 3535−3546.
(19) Alman, D. E. Reactive sintering of TiAl−Ti_5Si_3 in situ composites. *Intermetallics* **2005**, *13*, 572−579.
(20) Yeh, C. L.; Su, S. H. In situ formation of TiAl−TiB_2 composite by SHS. *J. Alloys Compd.* **2006**, *407*, 150−156.
(21) Shu, S.; Xing, B.; Qiu, F.; Jin, S.; Jiang, Q. Comparative study of the compression properties of TiAl matrix composites reinforced with nano-TiB_2 and nano-Ti_5Si_3 particles. *Mater. Sci. Eng., A* **2013**, *560*, 596−600.
(22) Qiu, F.; He, Y.; Zhu, L.; Shu, S.; Hu, W.; Zhan, C.; Jiang, Q. Microstructure and compression properties of in situ dual phase nanosized (TiB_2−Ti_5Si_3)/TiAl matrix composites fabricated by combustion synthesis and hot press consolidation. *Powder Metall.* **2015**, *58*, 235−240.
(23) Zhang, J.; Liu, L.; Wang, L.; Jiang, W.; Chen, L.; Tu, R.; Goto, T. Microstructures and mechanical properties of TiN-TiB_2-Ti_5Si_3 composites in-situ fabricated by spark plasma sintering. *J. Ceram. Soc. Jpn.* **2009**, *117*, 1085−1088.
(24) Jain, D.; Reddy, K. M.; Mukhopadhyay, A.; Basu, B. Achieving uniform microstructure and superior mechanical properties in ultrafine grained TiB_2−$TiSi_2$ composites using innovative multi stage spark plasma sintering. *Mater. Sci. Eng., A* **2010**, *528*, 200−207.
(25) Murthy, T. S. R. C.; Subramanian, C.; Fotedar, R. K.; Gonal, M. R.; Sengupta, P.; Kumar, S.; Suri, A. K. Preparation and property evaluation of TiB_2+$TiSi_2$ composite. *Int. J. Refract. Hard Met.* **2009**, *27*, 629−636.
(26) Raju, G. B.; Basu, B. Densification, sintering reactions, and properties of titanium diboride with titanium disilicide as a sintering aid. *J. Am. Ceram. Soc.* **2007**, *90*, 3415−3423.
(27) Evtushok, T. M.; Gordienko, S. P. Thermodynamic Analysis of High-Temperature Oxidation of Material in the Cr−TiB_2−$TiSi_2$ System in Air. *Powder Metall. Met. Ceram.* **2004**, *43*, 280−283.
(28) Karthiselva, N. S.; Murty, B. S.; Bakshi, S. R. Low temperature synthesis of dense TiB_2 compacts by reaction spark plasma sintering. *Int. J. Refract. Hard Met.* **2015**, *48*, 201−210.
(29) Wang, H. Y.; Lü, S. J.; Xiao, W.; Liu, G. J.; Wang, J. G.; Jiang, Q. C. Reaction Pathway of Combustion Synthesis of Ti_5Si_3 in Cu−Ti−Si System. *J. Am. Ceram. Soc.* **2013**, *96*, 950−956.
(30) Calka, A.; Oleszak, D. Synthesis of TiB_2 by electric discharge assisted mechanical milling. *J. Alloys Compd.* **2007**, *440*, 346−348.
(31) Yu, J.; Ma, L.; Abbas, A.; Zhang, Y.; Gong, H.; Wang, X.; Zhou, L.; Liu, H. Carbothermal reduction synthesis of TiB_2 ultrafine powders. *Ceram. Int.* **2016**, *42*, 3916−3920.
(32) Ma, L.; Yu, J.; Guo, X.; Xie, B.; Gong, H.; Zhang, Y.; Zhai, Y.; Wu, X. Preparation and sintering of ultrafine TiB_2 powders. *Ceram. Int.* **2018**, *44*, 4491−4495.
(33) Kang, S. H.; Kim, D. J. Synthesis of nano-titanium diboride powders by carbothermal reduction. *J. Eur. Ceram. Soc.* **2007**, *27*, 715−718.
(34) Yu, J.; Ma, L.; Zhang, Y.; Gong, H.; Zhou, L. Synthesis of TiB_2 powders via carbothermal reduction of TiO_2, HBO_2 and carbon black. *Ceram. Int.* **2016**, *42*, 5512−5516.
(35) Huang, B.; Chen, S.; Yao, Z.; Zhang, M.; Jing, Y.; Li, B.; Xiong, W. Study of carbothermal synthesis of TiB_2 assisted by extended high-energy milling. *Powder Technol.* **2015**, *275*, 69−76.
(36) Welham, N. J. Formation of TiB_2 from rutile by room temperature ball milling. *Miner. Eng.* **1999**, *12*, 1213−1224.
(37) Welham, N. J. Formation of nanometric TiB_2 from TiO_2. *J. Am. Ceram. Soc.* **2000**, *83*, 1290−1292.
(38) Bao, K.; Wen, Y.; Khangkhamano, M.; Zhang, S. Low-temperature preparation of titanium diboride fine powder via magnesiothermic reduction in molten salt. *J. Am. Ceram. Soc.* **2017**, *100*, 2266−2272.
(39) Mousavian, R. T.; Sharafi, S.; Shariat, M. H. Microwave-assisted combustion synthesis in a mechanically activated Al−TiO_2−H_3BO_3 system. *Int. J. Refract. Hard Met.* **2011**, *29*, 281−288.
(40) Nozari, A.; Heshmati-Manesh, S.; Ataie, A. A facile synthesis of TiB_2 nano-particles via mechano-thermal route. *Int. J. Refract. Hard Met.* **2012**, *33*, 107−112.
(41) Chen, Z.; Morita, K. *Reduction of titanium bearing slag to titanium silicide*; Presented in part at the 170th ISIJ Conference, Fukuoka, Japan, Sept 2015.
(42) Chen, Z.; Li, Y.; Tan, Y.; Morita, K. Reduction of Titanium Oxide by Molten Silicon to Synthesize Titanium Silicide. *Mater. Trans.* **2015**, *56*, 1919−1922.
(43) Chen, Z.; You, Y.; Morita, K. Synthesis and Kinetics of Titanium Silicides from Photovoltaic Industry Waste and Steelmaking Slag for Silicon and Titanium Recovery. *ACS Sustainable Chem. Eng.* **2018**, *6*, 7078−7085.
(44) Mills, K. C.; Yuan, L.; Jones, R. T. Estimating the physical properties of slags. *J. South. Afr. Inst. Min. Metall.* **2011**, *111*, 649−658.
(45) Sasaki, H.; Tokizaki, E.; Terashima, K.; Kimura, S. Density variation of molten silicon measured by an improved Archimedian method. *Jpn. J. Appl. Phys.* **1994**, *33*, 3803.
(46) Rosenkranz, R.; Frommeyer, G.; Smarsly, W. Microstructures and properties of high melting point intermetallic Ti_5Si_3 and $TiSi_2$ compounds. *Mater. Sci. Eng., A* **1992**, *152*, 288−294.
(47) Langen, M.; Hibiya, T.; Eguchi, M.; Egry, I. Measurement of the density and the thermal expansion coefficient of molten silicon using electromagnetic levitation. *J. Cryst. Growth* **1998**, *186*, 550−556.
(48) Meng, L.; Zhong, Y.; Wang, Z.; Chen, K.; Qiu, X.; Cheng, H.; Guo, Z. Supergravity separation for Cu recovery and precious metal concentration from waste printed circuit boards. *ACS Sustainable Chem. Eng.* **2018**, *6*, 186−192.
(49) Kubíček, P.; Pepřica, T. Diffusion in molten metals and melts: application to diffusion in molten iron. *Int. Met. Rev.* **1983**, *28*, 131−157.
(50) Wang, L.; Cui, Y.; Yang, J.; Zhang, C.; Cai, D.; Zhang, J.; Sasaki, Y.; Ostrovski, O. Melting Properties and Viscosity of SiO_2-CaO-Al_2O_3-B_2O_3 System. *Steel Res. Int.* **2015**, *86*, 670−677.
(51) Zhang, Z. T.; Sridhar, S.; Cho, J. W. An investigation of the evaporation of B_2O_3 and Na_2O in F-free mold slags. *ISIJ Int.* **2011**, *51*, 80−87.
(52) Dumay, C.; Cramb, A. Density and interfacial tension of liquid Fe-Si alloys. *Metall. Mater. Trans. B* **1995**, *26*, 173−176.
(53) Gómez, H.; Calo, V. M.; Bazilevs, Y.; Hughes, T. J. Isogeometric analysis of the Cahn−Hilliard phase-field model. *Comp. Method Appl. Mech. Eng.* **2008**, *197*, 4333−4352.
(54) Sato, Y.; Kameda, Y.; Nagasawa, T.; Sakamoto, T.; Moriguchi, S.; Yamamura, T.; Waseda, Y. Viscosity of molten silicon and the factors affecting measurement. *J. Cryst. Growth* **2003**, *249*, 404−415.
(55) Fujii, H.; Matsumoto, T.; Nogi, K.; Hata, N.; Nakano, T.; Kohno, M. Surface tension of molten silicon measured by the electromagnetic levitation method under microgravity. *Metall. Mater. Trans. A* **2000**, *31*, 1585−1589.
(56) Gao, Y.; Bian, L.; Liang, Z. Influence of B_2O_3 and TiO_2 on Viscosity of Titanium-Bearing Blast Furnace Slag. *Steel Res. Int.* **2015**, *86*, 386−390.
(57) Ren, S.; Zhang, J.; Wu, L.; Liu, W.; Bai, Y.; Xing, X.; Su, B.; Kong, D. Influence of B_2O_3 on viscosity of high Ti-bearing blast furnace slag. *ISIJ Int.* **2012**, *52*, 984−991.
(58) Wang, Z.; Shu, Q.; Chou, K. Viscosity of Fluoride-Free Mold Fluxes Containing B_2O_3 and TiO_2. *Steel Res. Int.* **2013**, *84*, 766−776.
(59) Girifalco, L.; Good, R. A theory for the estimation of surface and interfacial energies. I. Derivation and application to interfacial tension. *J. Phys. Chem.* **1957**, *61*, 904−909.
(60) Li, J.-G.; Hausner, H. Wetting and infiltration of graphite materials by molten silicon. *Scr. Metall. Mater.* **1995**, *32*, 377−382.
(61) Sahajwalla, V.; Khanna, R.; Mehta, A. Influence of chemical compositions of slag and graphite on the phenomena occurring in the graphite/slag interfacial region. *Metall. Mater. Trans. B* **2004**, *35*, 75−83.

DOI: 10.1021/acssuschemeng.8b02058
ACS Sustainable Chem. Eng. 2018, 6, 10742−10750

(62) Shen, P.; Fujii, H.; Nogi, K. Wettability of some refractory materials by molten SiO_2−MnO−TiO_2−FeO_x slag. *Mater. Chem. Phys.* **2009**, *114*, 681−686.

NOTE ADDED AFTER ASAP PUBLICATION

The wrong affiliation was marked for the third author in the version published ASAP on July 10, 2018. The corrected version was published on July 12, 2018.

DOI: 10.1021/acssuschemeng.8b02058
ACS Sustainable Chem. Eng. 2018, 6, 10742−10750